Manuscript(For revision, upload clean version of revised paper) Click here to view linked References

Fracture behavior of rammed earth in historic buildings

Ignacio Arto[a], Rafael Gallego[a], Héctor Cifuentes[b], Esther Puertas[a], Lourdes Gutiérrez-Carrillo[c].

[a] Dept. of Structural Mechanics and Hydraulic Engineering, University of Granada, Avda. Fuentenueva, 18001 Granada, Spain.

[a] Dept. of Continuum Mechanics and Theory of Structures, University of Sevilla, C. de los Descubrimientos, s/n. Pabellón Pza. de América, 41092 Sevilla, Spain.

[a] Dept. of Architectural Construction, University of Granada, Avda. Fuentenueva, 18001 Granada, Spain.

Abstract.

Rammed earth is the construction system of many heritage structures and buildings in different regions of the planet, some of which are seismically active areas. For this reason, these historic buildings can sustain structural damage or have already been subjected to stresses that have led to high levels of cracking in the rammed earth walls. Therefore, knowledge of the fracture behavior of this material is essential to assess the actual state of structural safety and the remaining mechanical capacity. The number of studies on the fracture behavior of rammed earth is limited, and even fewer studies have considered lime as a stabilizer and used traditional materials. This study measured the density, ultrasonic pulse velocity, fracture energy and tensile strength of prismatic specimens with two different soil: lime dosages and found relationships between the different parameters analyzed and the dosages used. Finally, it was verified that the fracture behavior of rammed earth can be assumed to be similar to that of mass concrete from a qualitative standpoint. For this reason, rammed earth could be considered as a quasi-brittle material that follows Hillerborg's discrete crack model.

Highlights.

- The influence of dosage on the density and ultrasonic pulse velocity of rammed earth test tubes was analyzed.
- The fracture energy and tensile strength values are related to the dosage of the specimens.
- Rammed earth could be considered as a quasi-brittle material that follows Hillerborg's discrete crack model.

Keywords. Rammed earth, fracture behavior, ultrasonic test, historical structures

1. Introduction.

Rammed earth (RE) is a common construction system based on load-bearing wall structures, with examples found in all continents. From the Neolithic revolution to the 20th century, many cultures have used this system in their residential and heritage buildings, incorporating local and traditional solutions that turn these structures into vernacular architecture elements [1-3]. Different and distant cultures such as the Roman, Chaldean, Yangshao and Incan cultures frequently used soil as a construction material. From the historical and patrimonial perspectives, structures made of RE represent more than 10% of the assets declared as Cultural Heritage of Humanity by UNESCO [4]. Some unique and emblematic examples are the historic center of the city of Lyon, the Lasha palaces in Tibet, the Great Wall of China, the Alhambra in Granada or the citadel of Bam in Iran. The latter had the highest density of buildings made with soil in the world until a 6.5 magnitude earthquake destroyed 80% of its structures on December 26, 2003 [5]. As in this case, many of the heritage structures built with RE are located in high seismic hazard areas, and consequently, the risk of destruction and loss is very high.

Because these are historic structures that have existed for a long time, many of them have been affected by past earthquakes of varying intensities. For this reason, it is very likely that in its current state of conservation, RE has internal or external cracks that will result in fractures, which may or may not be visible, and is in no way similar to homogeneous and continuous materials. Therefore, knowledge of the fracture behavior of RE is necessary to accurately assess its current state. In addition, knowledge of the actual remaining capacities of existing structures is essential for analyzing the risks of heritage buildings exposed to seismic or other stresses. Thus, characterization of the fracture behavior is one of the fields with the most potential for this type of material.

In addition, RE is a material that offers great environmental advantages because structures made with it have a very low carbon footprint due to various favorable circumstances. Soil, as a basic material, is very abundant and easy to obtain. Its availability in the same place where a building is to be erected makes the need to move it over long distances unnecessary, and this reduces energy expenditure in transport. In addition, the technology and auxiliary means used to raise RE walls are very simple and reusable and rely on natural materials based on the use of simple wooden boards as formwork and rammers made of wood or stone [6-8]. Furthermore, at the end of their useful life, RE structures are easily removable, and the material that constitutes their walls is directly returned to the land without generating construction waste. Toxic or polluting materials are also not used during its manufacture; therefore, no hazardous waste is generated.

Finally, it should be mentioned that the thickness of RE walls, together with the low thermal conductivity of soil, allows buildings constructed with this technique to maintain very stable interior thermal conditions. For this reason, these dwellings require very little energy to achieve adequate levels of thermal comfort, which also reduces their environmental impact [9].

Domestic buildings made with RE, despite their great use, have a link to poverty because on many occasions, the use of RE is based on a shortage of materials or economic means. Additionally, it is clear when looking at many heritage buildings, that RE structures can have a very long useful life if they are well built and maintained. Therefore, to increase the social acceptance of this type of material, it is necessary to explain their medium-term environmental and economic advantages and to study their weaknesses at a mechanical level to improve them and achieve stronger structures [10].

To date, most of the research on the mechanical capacities of RE have focused on the improvement of these capacities through various strategies. Numerous studies can be found in which the authors increase these capacities with the addition of both textile and natural fibers, glass or plastic inside [11-17] as well as outside [18] the material. The results of these studies vary, and it is difficult to compare these studies due to the different materials, RE compositions and types of tests used. Another strategy used is the addition of stabilizers to the RE mass. Only a few authors have researched the capacities of the material in its simplest form, which is a mixture of soil with aggregates and water, without any type of stabilizer [19-21]. The main stabilizer used in previous research is cement [12,13,15-17,22-25], while a smaller number of studies have used lime [26,27] or various materials such as pozzolans or guar gum [16]. Historic RE buildings have almost exclusively used lime as a stabilizer, either in the form of aerial lime or natural hydraulic lime [28-31]. There are also references to the historical use of animal products such as blood, urine or manure with stabilizing functions [32]. Their use improved the mechanical behavior and workability of RE during its manufacture.

When using lime-stabilized specimens, one of the factors to consider in order to obtain specimens with the most similar characteristics possible is the carbonation rate. The lime used to produce the specimens, which is present in the form of calcium hydroxide, $Ca(OH)_2$, requires a certain amount of time to eliminate one water molecule and incorporate atmospheric CO_2 until it once again becomes the original calcium carbonate, $CaCO_3$. Therefore, depending on the amount of time elapsed, the amount of calcium carbonate inside a specimen will increase until the entire section is completed. As with concrete, the carbonation rate depends on several factors, such as porosity, the amounts of lime and mixing water, compaction and environmental conditions [33,34].

In regards to the assessment of the nonlinear mechanical capacities of RE, we should point out that very few studies have focused on its fracture behavior, and even fewer studies have characterized its value for heritage materials. Most of the authors have used the wedge splitting test (WST), with some variations to adapt it to the material [13,16], but all of them have used cement as a stabilizer, thus moving away from historical RE materials. Very few authors have used the three-points bending test (3PBT) [20], and no studies have used this type of test on specimens stabilized with lime. The aim of the present study was to understand the behavior of RE stabilized with lime in a nonlinear regime, by imitating traditional materials, dosages and forms of execution that are found in existing heritage structures. To this end, fracture energy values and their softening law

were obtained through 3PBT tests, and qualitative relationships with other more studied materials such as mass concrete were established.

During the curing period of the specimens, from their manufacture to the 3PBT tests, data were collected systematically to learn the weight and density changes experienced. To do this, the moisture loss in the specimens and the variation in the propagation velocity of ultrasonic pulses were controlled throughout the curing period. The number of studies on the behavior of the velocity of an ultrasonic pulse (UPV) in RE is also limited. This nondestructive evaluation technique has been used by several authors to obtain relationships between the mechanical and physical parameters of the materials used in historical structures or to evaluate the differences between different dosages, degrees of humidity, stabilizers or additives [27,35-37]. By controlling the variation in the moisture loss and the ultrasonic pulse velocity, a minimum curing period was established in which the physical and mechanical characteristics of the specimens varied, regardless of carbonation. Once these two parameters were stable, the specimens reached maturity and were subjected to mechanical tests.

2. Materials and methods.

The soil selected to produce the specimens analyzed in this paper was from a quarry in the vicinity of the city of Granada (Spain), had a maximum aggregate size of less than 10 mm and a chloride and sulfate content of less than 0.002% and was free of organic matter and light contaminants. A natural hydraulic lime (NHL) 3.5, which is the product of the calcination of a marly limestone that has been subsequently slaked, was used as a stabilizer. Figure 1 shows the granulometric curve of the material used and the curves obtained from existing RE in walls and castles built between the XI and XIV centuries in Granada (Gr) [38] and in the walls of San Juan de Aznalfarache, which was built in the XII century in the city of Seville (Se) [39].

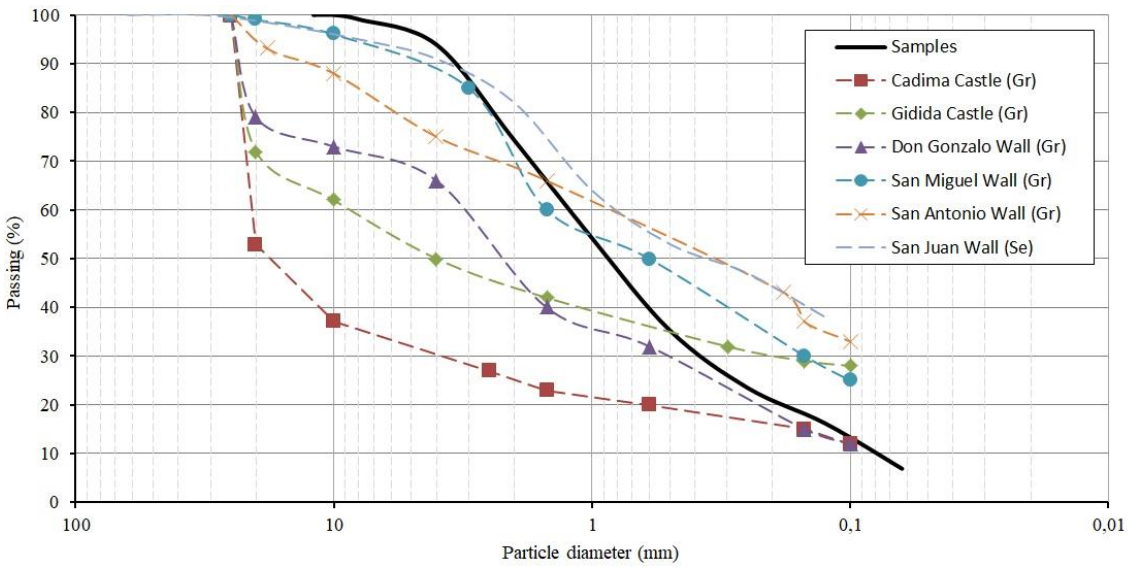

Fig. 1. Particle grading curves for RE.

The soil was mixed in 3:1 and 4:1 ratios with lime as a stabilizer (parts of aggregate:lime), with 13% mixing water added as a percentage of weight. The ratios were taken from the dosage data of two samples extracted from the Alhambra in Granada (XIII-XIV centuries) [40], where the aggregate:lime ratios are between 73% and 84% of aggregate versus 27% and 16% of binder, which are comparable to 3:1 and 4:1 ratios, respectively. Cement was not used as a stabilizer due to the problems of molecular incompatibility with clays, the petrophysical level (high microporosity of the hardened cement) and the possible presence of sulfates in the cement, which can cause soluble salts to appear and alter the cement-soil system [41-46], in addition to differing from historical solutions and materials [47]. With these dosages, twelve prismatic 440x100x100 mm specimens were made with the cross section size indicated in RILEM for an aggregate diameter of less than 10 mm [48].

The soil, lime and water were mixed manually until a homogeneous material was obtained. Once this process was finished, the material was poured into a wooden formwork in layers of 30 mm. Each layer was compacted manually until a final thickness of between 15 and 20 mm was reached; consequently, each specimen included 5 or 6 layers. Table 1 shows all the initial data of the specimens, divided into series of series A specimens, with a soil:lime dosage of 3:1, and series of series B specimens, with a 4:1 dosage. The average initial density of series A specimens was 2.15 g/cm^3, with a deviation of around ±1.2%, and the average initial weight was 10044 g, with a deviation between +1.55% and -2.17%. The average initial density of series B specimens was 2.18 g/cm^3, with a deviation lower than ±2.00%, and the average initial weight was 10138 g, with a deviation of around ±0.50%.

Table 1
Initial data of specimens. (Mean values in bold).
Series A – dosage 3:1

Specimen	Date	Dimensions (mm)			Volume (cm^3)	*Volume deviation*	Initial weight (g)	*Initial weight deviation*	Initial density (g/cm^3)	*Initial density deviation*
		length	height	width						
A1	2019-06-26	441.75	104.80	101.10	4680.46	*0.03%*	10149	*1.05%*	2.17	*1.09%*
A2	2019-05-15	443.00	103.01	101.18	4617.19	*-1.33%*	9970	*-0.73%*	2.16	*0.62%*
A3	2019-05-13	443.00	102.48	102.00	4630.66	*-1.04%*	10063	*0.19%*	2.17	*1.09%*
A4	2019-06-04	443.25	105.80	101.50	4759.93	*1.72%*	10001	*-0.42%*	2.10	*-2.17%*
A5	2019-06-04	443.25	105.45	101.28	4733.90	*1.17%*	9919	*-1.24%*	2.10	*-2.17%*
A6	2019-06-06	443.50	103.12	101.75	4653.41	*-0.55%*	10159	*1.15%*	2.18	*1.55%*
				mean	**4679.26**		**10044**		**2.15**	

Series B – dosage 4:1

Specimen	Date	Dimensions (mm)			Volume (cm^3)	*Volume deviation*	Initial weight (g)	*Initial weight deviation*	Initial density (g/cm^3)	*Initial density deviation*
		length.	height	width						
B1	2019-05-16	442.88	104.16	101.25	4670.70	*0.59%*	10101	*-0.36%*	2.16	*-1.07%*
B2	2019-06-03	443.80	103.26	101.08	4632.17	*-0.24%*	10133	*-0.05%*	2.19	*0.31%*
B3	2019-06-03	444.25	105.80	101.16	4754.69	*2.40%*	10189	*0.51%*	2.14	*-1.98%*
B4	2019-06-06	444.03	101.24	101.62	4568.18	*-1.62%*	10131	*-0.07%*	2.22	*1.68%*
B5	2019-06-07	443.10	102.91	101.45	4626.06	*-0.37%*	10172	*0.34%*	2.20	*0.76%*
B6	2019-06-07	444.50	102.31	101.32	4607.71	*-0.77%*	10100	*-0.37%*	2.19	*0.31%*
				mean	**4643.25**		**10138**		**2.18**	

The use of wooden formwork, which imitates traditional methods, caused slight variations in both the length and width of the specimens, although none of the specimens exceeded 1% of the established size. However, four of the specimens (A1, A4, A5 and B3) showed height variations of approximately 5%. The method used to produce the specimens, in which the layers are parallel to the longitudinal direction, requires visual control of the total height of the specimen, which caused these variations. Once produced, the specimens were kept in a laboratory environment (24ºC and 40% RH) until the 3PBT fracture tests were performed. The specimens were placed on metal frames to facilitate contact of the four faces with air and thus encourage equal carbonation in all faces. The curing conditions were controlled at all times to obtain specimens that were subjected to the same conditions as the real structures. Figure 2 shows the process of producing the specimens and the storage and curing process in laboratory conditions.

Fig. 2. Production of specimens (left) and storage and curing process in the laboratory (right).

The depth of carbonation in the lime-stabilized specimens should be controlled because the recovery of ambient CO_2 in the lime cycle increases its resistance. In our case, a specific specimen was used to measure the carbonation progress over a given

period of time. The carbonation state of the rest of the specimens on the date of the fracture tests was thereby inferred.

The method to produce the specimens and the subsequent tests carried out on them were designed simulate the conditions of a typical section located inside a wall (Figure 3). The method to produce the specimens involved reproducing the arrangement of the layers and the construction direction of an actual wall, which is upward, and the accessible wall fronts, exterior face and interior face. It is on these accessible faces that the probes for UPV tests could be placed, such that the ultrasonic pulse moved in parallel to the layers along the thickness of the theoretical wall. This is how the UPV tests were carried out on the specimens.

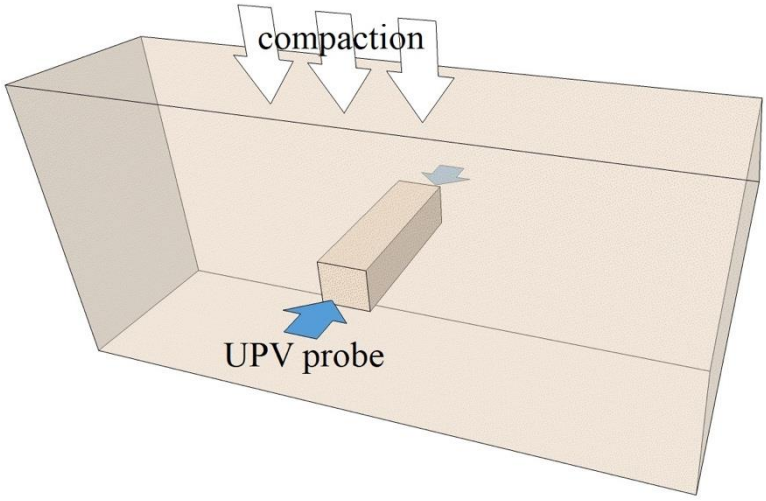

Fig. 3. Simulation of the location of a probe inside a wall. Compaction direction and position of the accessible faces for the placement of probes in the UPV tests.

The evolution of the weight of the specimens was controlled for at least 30 days after their production. An Ohaus GEO15 precision balance was used. The time required to obtain specimens with a stable density and water content was verified once all the mixing water had been balanced with the ambient moisture or permanently incorporated into the material.

The evolution of the UPV was measured with a Controls brand ultrasonic tester model 58-E0048, with a frequency range of 54kHz following standard UNE-EN 12504-4 [49]. Data were collected from the samples during the 28 days after the specimens were produced, which confirmed an increase in the UPV related to moisture loss and stabilizer setting. A longer study was not carried out because, as shown below, starting at 15 days after the specimens were produced, the UPV values became stable.

To determine the fracture energy, 3PBT tests were carried out on the specimens after making a notch of 1/6 of the height of the specimen. This notch was made by cutting with a disk saw. The procedure used to obtain the specific energy was the work-of-fracture method [48], with the corrections proposed by other authors [50-52].

The test was carried out by controlling the crack mouth opening with a clamp transducer. In addition, the vertical displacement of the cross section of the specimen was measured with an inductive linear transducer mounted on a rigid frame coupled to the specimen. The supports and the load application system were anti-torsion to avoid parasitic torsions. Figure 4 shows a picture of one of the 3PBT tests. The weight of the specimen was compensated for by using elastic bands.

Fig. 4. Three-point bending test of the specimens.

3. Results.

3.1. Results of controlling the weight evolution of the specimens.

The behavior of the water inside the specimens that was incorporated during mixing was controlled. To do this, the weight variation was checked for at least 30 days. Figure 5 shows the percentage of the accumulated moisture loss from the moment the specimens were produced and the mean of each series depending on the soil:lime ratio (3:1 and 4:1).

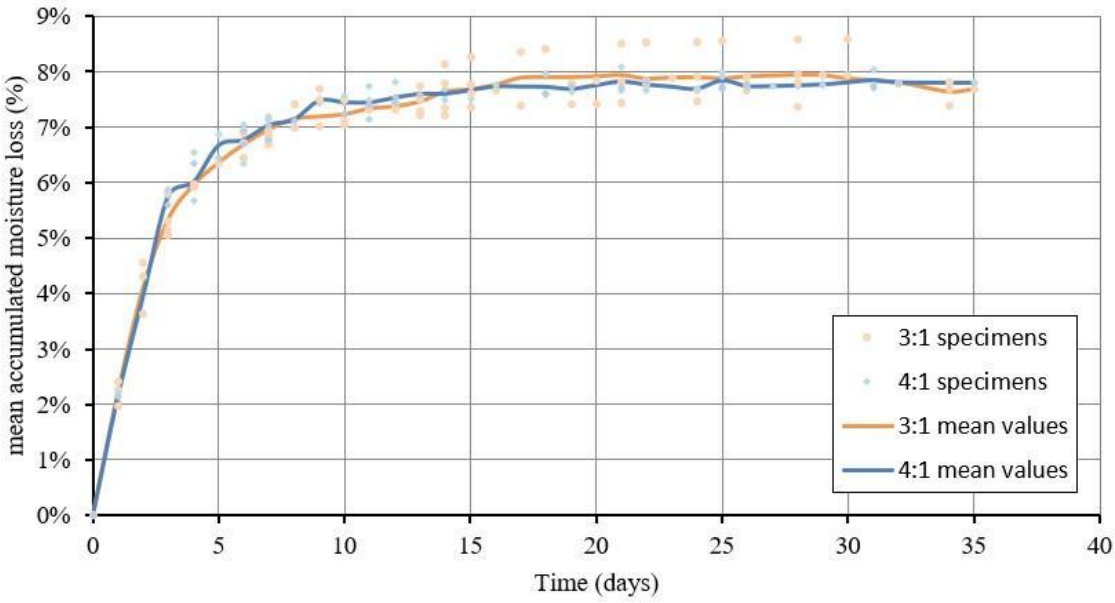

Fig. 5. Specimens and mean accumulated moisture loss (%).

The results indicate that the moisture loss was highly accelerated during the first days for both dosages and stabilized from day 15 onwards, with accumulated values approximately 7.66%. After that point, the rate of moisture loss became much slower, with a small increase in the following two weeks until a final accumulated mean value of 7.84%. Different behaviors were not observed in the two dosages, and the curves representing the means of both practically coincide.

3.2. Results of controlling the evolution of the ultrasonic pulse velocity (UPV).

The evolution of the propagation velocity of an ultrasonic pulse inside the specimens during the 28 days after their manufacture was also controlled. Early control of these data provides an idea about the behavior of the water inside the specimens and the setting speed, which is ultimately related to the density of the material. The probes were placed on the end faces, with a separation of 440 mm, as would be done on a real wall of that thickness. Figure 3 shows the arrangement; thus, the pulse advances parallel to the layers along the thickness of a theoretical wall. The behavior of an ultrasonic pulse perpendicular to the layers was not studied because this situation cannot be measured in actual structures, and it has been studied by other authors [27].

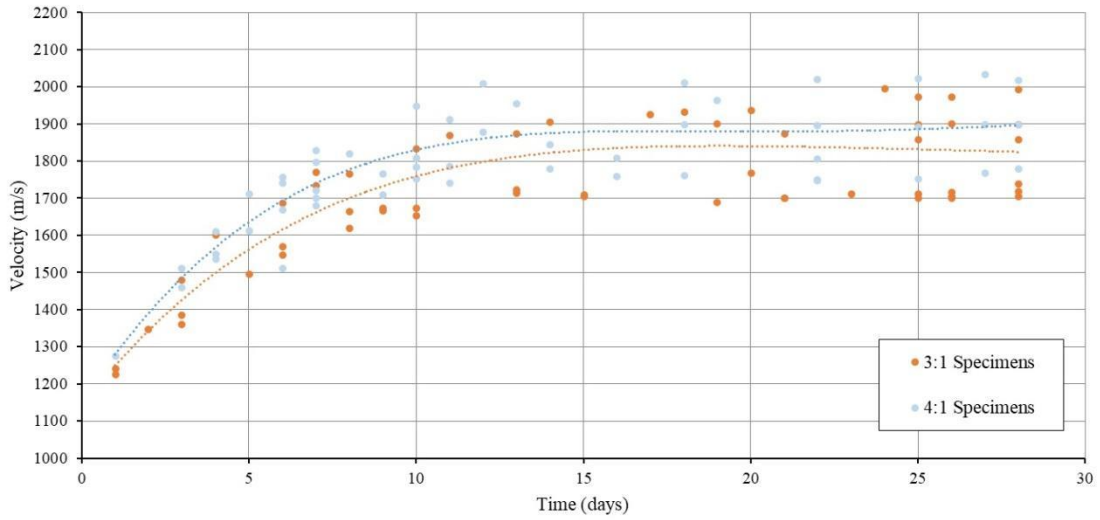

Fig. 6. UPV specimen values and mean curve for each dosage (m/s).

Figure 6 shows the UPV values measured on the specimens for 28 days and the curve of their mean trend. This figure shows that the 3:1 dosage presented values at 28 days of approximately 1830 m/s, while the 4:1 dosage reached a mean value of 1885 m/s. The difference represents an insignificant increase of 3%, although the specimens with a lower quantity of lime tended to have the highest values. Figure 6 also shows how starting at day 15, the UPV values became stable, without significant variations in the remaining days.

A review of the increase in the UPV during the 28 days shows that both dosages had the same behavior. Figure 7 shows the accumulated increases in the UPV during the test period. It was observed that the increase in the accumulated velocity was 27.52% on average between both dosages in the first five days. It was 12.20% over the next five days until day 10, and then in the next five days, it increased another 3.19% until day 15. From that moment forward, the increase was only 0.44%. Finally, the total accumulated UPV increase from the beginning to the end of the test was 43.21%.

Table 2 summarizes the density and UPV data of the specimens at 28 days of age. The series A specimens had a mean density of 1.98 g/cm^3, with deviations below ± 2.00%, and a mean UPV value of 1818.16 m/s, with deviations between + 9.59% and -6.22%. At the same time, the series B specimens had a mean density of 2.01 g/cm^3, with deviations around ± 1.50%, and a mean UPV value of 1869.36 m/s, with deviations between + 7.98% and - 6.44%.

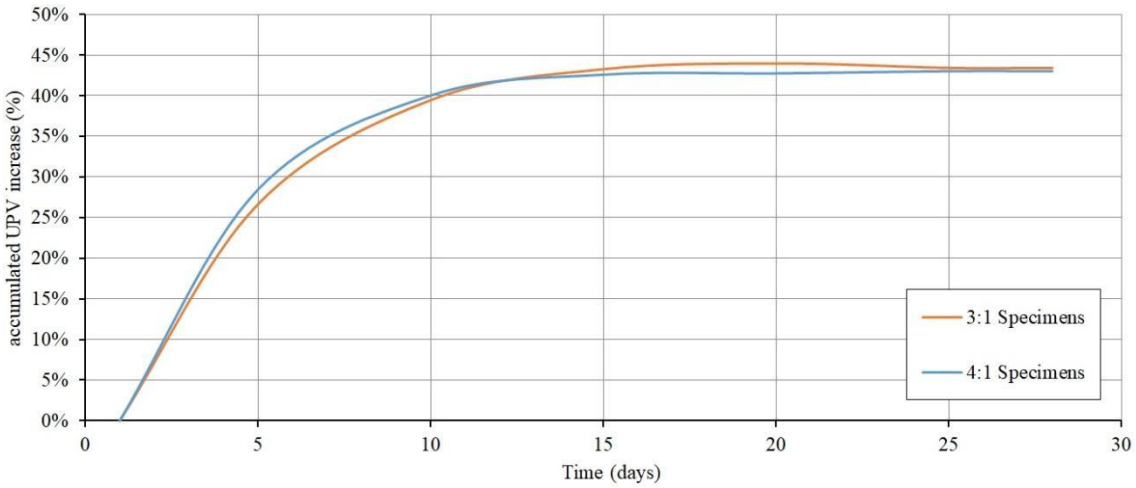

Fig. 7. UPV increase for each dosage (%).

Table 2
Summary data for the specimens. (Mean values in bold).

Series A - 3:1 dosage

Specimen	Date	Final density (g/cm^3)	*Final density deviation*	Velocity (m/s)	*Velocity deviation*
A1	2019-07-24	2.00	*1.10%*	1992.50	*9.59%*
A2	2019-06-14	1.99	*0.59%*	1737.94	*-4.41%*
A3	2019-06-12	1.99	*0.59%*	1855.89	*2.08%*
A4	2019-07-02	1.94	*-1.94%*	1705.00	*-6.22%*
A5	2019-07-02	1.94	*-1.94%*	1718.23	*-5.50%*
A6	2019-07-04	2.01	*1.60%*	1899.39	*4.47%*
	mean	**1.98**		**1818.16**	

Series B - 4:1 dosage

Specimen	Date	Final density (g/cm^3)	*Final density deviation*	Velocity (m/s)	*Velocity deviation*
B1	2019-06-15	1.99	*-1.08%*	1777.90	*-4.89%*
B2	2019-07-01	2.02	*0.41%*	1748.92	*-6.44%*
B3	2019-07-01	1.98	*-1.57%*	1807.36	*-3.32%*
B4	2019-07-04	2.04	*1.41%*	1964.73	*5.10%*
B5	2019-07-05	2.02	*0.41%*	1898.64	*1.57%*
B6	2019-07-05	2.02	*0.41%*	2018.59	*7.98%*
	mean	**2.01**		**1869.36**	

3.3. Calculation of carbonation in the specimens.

To determine the depth of carbonation of the specimens, a control specimen with a 3:1 dosage was fractured after 48 days to measure the carbonation front. From these data and using the expression (1) [53], we estimated the carbonation depth in the

specimens on the date of the fracture tests. Expression (1) relates the carbonation depth (x) with the carbonation rate of the material (k) and the time (t).

$$x = k \cdot \sqrt{t} \qquad (1)$$

Thus, the control specimen was split at 48 days and the carbonation front was measured clearly by using a pH indicator. In this case, phenolphthalein dissolved at 1% in 95% ethanol was used. The measurement indicates a carbonation depth of 19.42 mm, as shown in Figure 8. With the carbonation depth (x) and time (t) data, the carbonation rate of the material (k) was obtained according to expression (1). Once the value of k (equal to 2.803) was obtained, the depth of the carbonation front of the specimens was calculated as a function of the elapsed time, as shown in Figure 9. This figure confirms that complete carbonation of the specimens (x = 50 mm) started to occur at 318 days after their manufacture. This is an extremely long wait period for research; thus, the decision was made to use specimens with 90% carbonation, which occurred at 130 days.

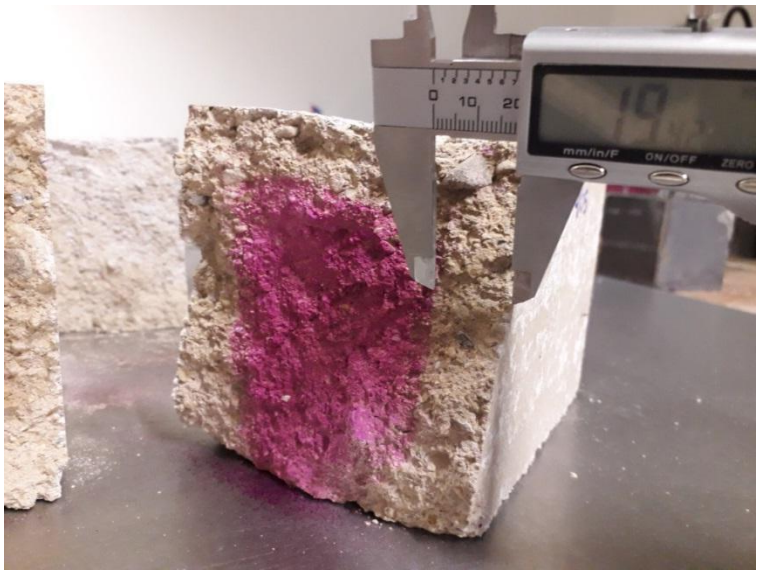

Fig. 8. Carbonation front measured on the control specimen at 48 days (19.42 mm).

The study specimens were subjected to fracture tests between 145 and 160 days from their manufacture, which implied a carbonation depth of approximately 35 mm and an uncarbonated section of less than 10%. It must be considered that carbonation advances on the four faces of a specimen, and therefore, a carbonation front of 35 mm implies a noncarbonated inner section of 30 x 30 mm^2, compared to the initial section of 100 x 100 mm^2. It would be interesting to conduct a larger study that relates the influence of carbonation to the mechanical performance of RE.

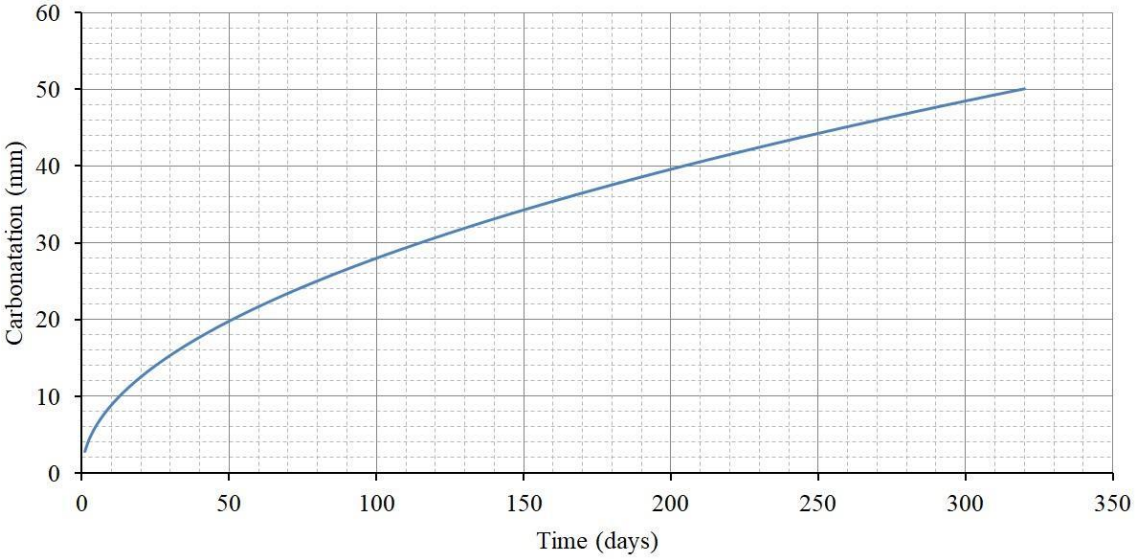

Fig. 9. Carbonation rate curve of the specimens.

3.4. Fracture behavior and fracture energy.

3PBT tests were performed on the previously notched specimens to determine the fracture energy. The depth of the notch was 1/6 of the height of the specimen and was made by cutting with a disk saw. Table 3 shows the dimensional values used to perform the test, and Figure 10 shows a schematic diagram of the dimensions. Specifically, the values for the width (B), height (D) and notch depth (a_0) of the specimen are shown, where A_{lig} is the narrowed area that remains after making the notch.

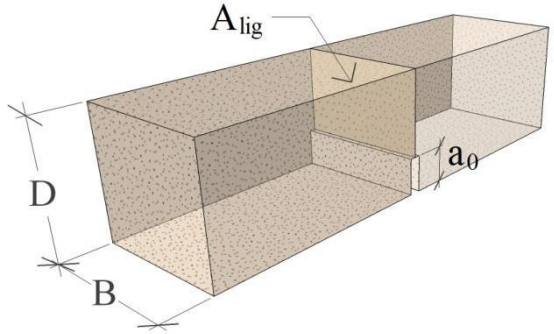

Fig. 10. Specimen dimensions.

Table 3 also includes the calculated work of fracture W_F values, which is the area under the load-displacement curve (P-δ) obtained during the test. The work of fracture measured on the load-displacement curve and the unmeasured work of fracture, obtained with the curve tail fitting procedure, are included. Finally, the value of the specific fracture energy (G_F) was calculated according to expression (2). The data and results obtained from the test are shown for each of the specimens, except for specimens A2, A4 and A5, which broke during handling or notching. The data of specimen B2 differ from

the data for the rest of the specimens; it was therefore considered to be an atypical case and eliminated from subsequent results.

$$G_F = \frac{W_F}{A_{lig}} \qquad (2)$$

Table 3.
Three-point bending test data. (Mean values in bold).

Serie A - dosage 3:1

Specimen	Section (mm)		a_0 (mm)	A_{lig} (mm^2)		W_F (Nm)	W_F *deviation*	G_F (N/m)	G_F *deviation*
	D. height	B. width							
A1	104.80	101.10	35	7057		0.215	*-9.15%*	30.47	*-10.25%*
A2	-	-	-	-		-	-	-	-
A3	102.48	102.00	37	6679		0.257	*8.59%*	38.48	*13.36%*
A4	-	-	-	-		-	-	-	-
A5	-	-	-	-		-	-	-	-
A6	103.12	101.75	32	7236		0.238	*0.56%*	32.89	*-3.11%*
					mean	**0.237**		**33.95**	

Series B - dosage 4:1

Specimen	Section (mm)		a_0 (mm)	A_{lig} (mm^2)		W_F (Nm)	W_F *deviation*	G_F (N/m)	G_F *deviation*
	D. height	B. width							
B1	104.16	101.25	34	7104		0.180	*10.02%*	25.34	*8.98%*
B2*	103.26	101.08	34	7001		0.083	-	11.86	-
B3	105.80	101.16	34	7263		0.148	*-9.54%*	20.38	*-12.36%*
B4	101.24	101.62	33	6935		0.152	*-7.09%*	21.92	*-5.72%*
B5	102.91	101.45	34	6991		0.153	*-6.48%*	21.89	*-5.87%*
B6	102.31	101.32	34	6921		0.185	*13.08%*	26.73	*14.97%*
					mean	**0.164**		**23.25**	

Figure 11 shows the fracture produced in specimen A1 after the test. On the left, the vertical trajectory of the fracture in the narrowed zone, from the notch to the point of application of the load, can be seen. The image on the right shows the inside of the material after the test. In this image, the cut zone of the notch can be clearly seen, with a smooth appearance unlike the rough area formed by the fracture during the test.

Fig. 11. Specimen A1. Detail of the fracture zone (left) and interior of the material after the test (right).

The shapes of the load-displacement curves are very similar to those obtained from testing mass concrete specimens. As an example, Figure 12 shows the P-δ curve for specimen A1.

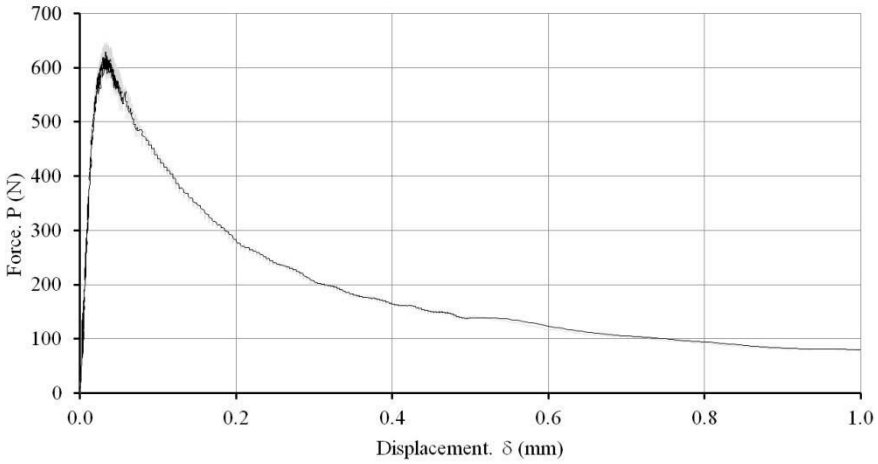

Fig. 12. Specimen A1. Force-displacement P-δ curve.

3.5. Fracture behavior and bilinear softening law.

In accordance with Hillerborg's discrete crack model [54], the law of cohesive stresses at the vertex of the crack was obtained using the hinge model [55]. The law is considered bilinear, as defined in Figure 13.

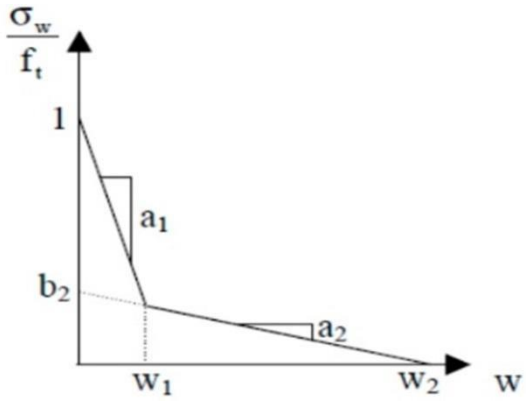

Fig. 13. Softening bilinear law [54].

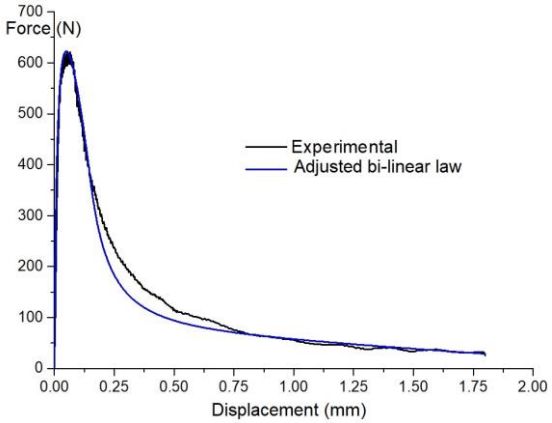

Fig. 14. Comparation between P-δ curve for specimen A6 and adjusted bilinear law.

As an example, Figure 14 shows the fit obtained for specimen A6 and a comparison with an adjusted bilinear law. It can be seen that the matching between the experimental and theoretical curves is fairly good. Table 4 shows the main parameters of the bilinear softening law obtained for each specimen.

Table 4
Softening bilinear values for each specimen (mean values in bold).

A series - dosage 3:1

Specimen	G_F (N/m)	f_t (Mpa)	*f_t deviation*	σ_1 (Mpa)	*σ_1 deviation*	a_1 (mm^{-1})	*a_1 deviation*	a_2 (mm^{-1})	*a_2 deviation*
A1	30.47	0.50	*2.74%*	0.06	*5.88%*	12	*9.09%*	0.041	*-20.65%*
A3	38.48	0.50	*2.74%*	0.05	*-11.76%*	11	*0.00%*	0.047	*-9.03%*
A6	32.89	0.46	*-5.48%*	0.06	*5.88%*	10	*-9.09%*	0.067	*29.68%*
	mean	**0.487**		**0.057**		**11**		**0.052**	

B series - dosage 4:1

Specimen	G_F (N/m)	f_t (Mpa)	*f_t deviation*	σ_1 (Mpa)	*σ_1 deviation*	a_1 (mm^{-1})	*a_1 deviation*	a_2 (mm^{-1})	*a_2 deviation*
B1	25.34	0.35	*-20.81%*	0.05	*0.00%*	12	*-16.67%*	0.060	*14.50%*
B3	20.38	0.45	*1.81%*	0.05	*0.00%*	15	*4.17%*	0.058	*10.69%*
B4	21.92	0.39	*-11.76%*	0.05	*0.00%*	15	*4.17%*	0.060	*14.50%*
B5	21.89	0.46	*4.07%*	0.05	*0.00%*	15	*4.17%*	0.042	*-19.85%*
B6	26.73	0.56	*26.70%*	0.05	*0.00%*	15	*4.17%*	0.042	*-19.85%*
	mean	**0.442**		**0.050**		**14**		**0.052**	

4. Discussion.

4.1. Relationship of the dosage with the moisture loss and UPV.

In regard to the moisture loss in the specimens, the results indicate that there do not seem to be differences in the behavior of the specimens depending on the dosage. The behavior of the twelve specimens is practically the same, with accelerated initial losses in the first five days, in which 83% of the total moisture loss took place. From that moment forward, the loss rate decreased until it was practically zero after day 15. This behavior was expected because the water that is not incorporated into the material and is on the surface of the specimen evaporates faster than the water inside, which must reach the surface to evaporate. These data may vary depending on the shape and volume/surface ratio of the specimen, among other factors.

The percentage of water used during the manufacture of the specimens was 13% of their weight, and the final loss was approximately 7.84%. Thus, the percentage of water finally incorporated into the material was approximately 5.16% (for laboratory conditions of 24ºC and 40% RH); this amount remained stable and was either trapped inside the specimen or became part of the chemical modifications suffered by the material components.

A similar behavior was observed in the fluctuations of the UPV measurements, with a similar evolution pattern. Thus, 63.69% of the final velocity increase accumulated in the first five days. This percentage dropped to 28.23% between days 5 and 10 and to 7.88% between days 10 and 15. From that day forward, the differences were approximately 1%. The fluctuation in the UPV seems to be related to the amount of water in the specimens; these both stabilize after 15 days from manufacture. Figure 6 shows that the UPV in the specimens with a 4:1 dosage is approximately 3% higher compared to the specimens with a 3:1 dosage. The increase is not very significant and seems to be more related to the density of the specimens than to the dosage, as shown in Figure 15. This figure also shows the increasing direction of the velocity-density relationship, which is similar to that of other types of materials such as mass concrete. As shown in Table 2, the densities of specimens B4, B5 and B6 are the highest overall, which is not related to the dosage but to a greater degree of compaction in their manufacture.

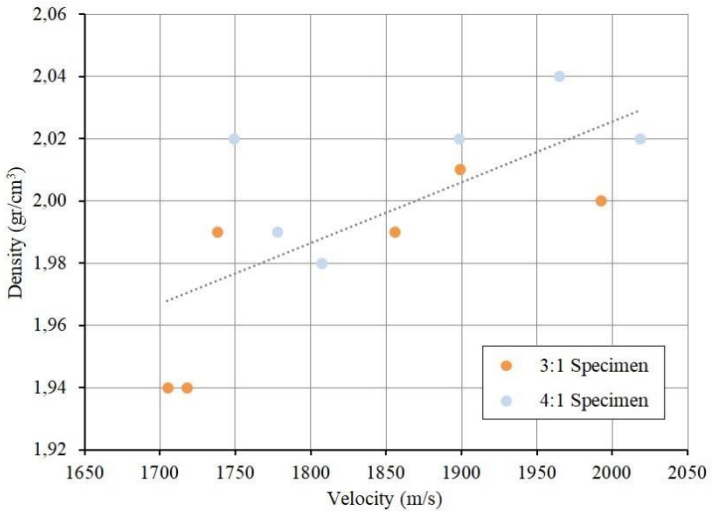

Fig. 15. Velocity (m/s) - density (gr/cm^3) relationship in the specimens.

By comparing the density and UPV mean results for the two dosages in Table 2 (Density$_{3:1}$ = 1.98 g/cm^3 UPV$_{3:1}$ = 1818.16 m/s; Density$_{4:1}$ = 2.01 g/cm^3 UPV$_{4:1}$ = 1869.66 m/s), it can be seen that the differences between the two are very small: 1.51% for the density and 2.83% for the velocity. These differences indicate that their values do not appear to be related to the dosage used.

4.2. Relationship between dosage and the G_F and f_t values.

Conversely to the fracture energy data obtained from the 3PBT tests, a clear difference is seen depending on the dosage. Thus, as shown in Table 3, for the dosage with the highest quantity of lime (3:1), the mean fracture energy is $G_{F\_3:1}$ = 33.95 N/m, with a deviation of around ±13%, while for the dosage with less lime (4:1), the mean fracture energy is $G_{F\_4:1}$ = 23.25 N/m, with a deviation of around ±15%. Therefore, by comparing the G_F data between both dosages, an increase of 46% is observed for the dosage with the higher lime quantity (3:1), which indicates a clear relationship between the G_F value and the dosage.

Regarding the effect of the dosage on the values of the softening law, the behavior observed is similar to that of the fracture energy. Thus, as shown in Table 4, the mean values of the tensile strength of the specimens with the 3:1 dosage reach values of $f_{t\_3:1}$ = 0.487 MPa, with a deviation of 5.48%, while for the 4:1 dosage, the values decrease to $f_{t\_4:1}$ = 0.442 MPa, with a deviation of around ±25.00%. These values represent a 10.18% increase in the tensile strength in the specimens with the greater amount of lime. This behavior is also in accordance with the increase in the initial slope a_1 of the bilinear cohesive law (Figure 13), where the value for the 3:1 dosage is $a_{1\_3:1}$ = 11 mm^{-1}, with a deviation of around ±9%, while for the 4:1 dosage it increases up to $a_{1\_4:1}$ = 14 mm^{-1}, with a deviation between +4% and -16.67%.

From the data, it can be seen how the higher G_F values relate to higher f_t values, as expected for this type of material. Figure 16 shows the trend of the simultaneous increase of both values, where the differences indicated above are maintained depending on the dosage.

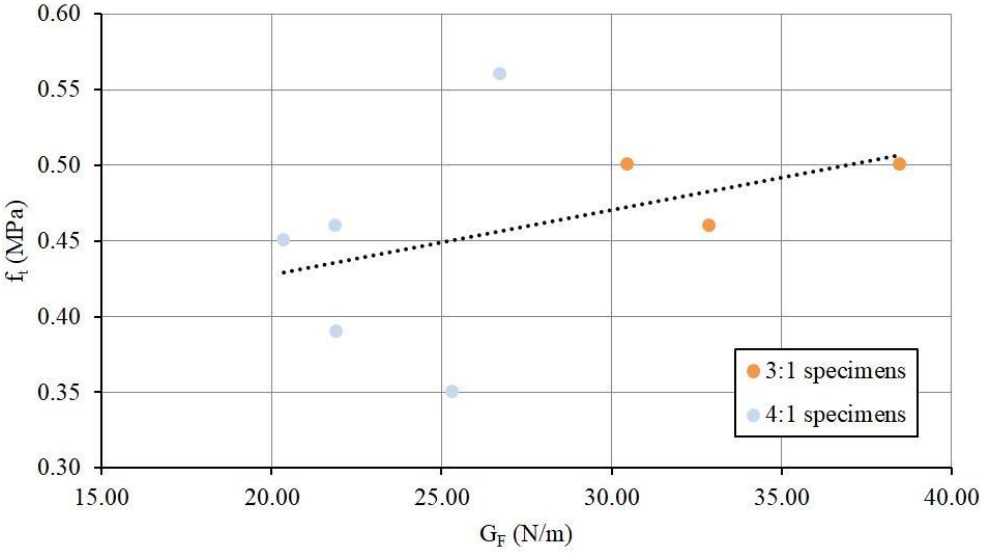

Fig. 16. Relationship between fracture energy G_F (N/m) and tensile strength f_t (MPa).

4.3. Relationship between UPV and the G_F and f_t values.

Once relationships between the material density and UPV values and between the fracture energy and tensile strength values were established, we related these two blocks to each other. Therefore, the relationships between the fracture energy and tensile strength values and the UPV values are shown below, revealing a relationship between the nonlinear mechanical parameters of the material and a nondestructive method. Different dosages were considered because it has been proven that the UPV is not related to the dosage.

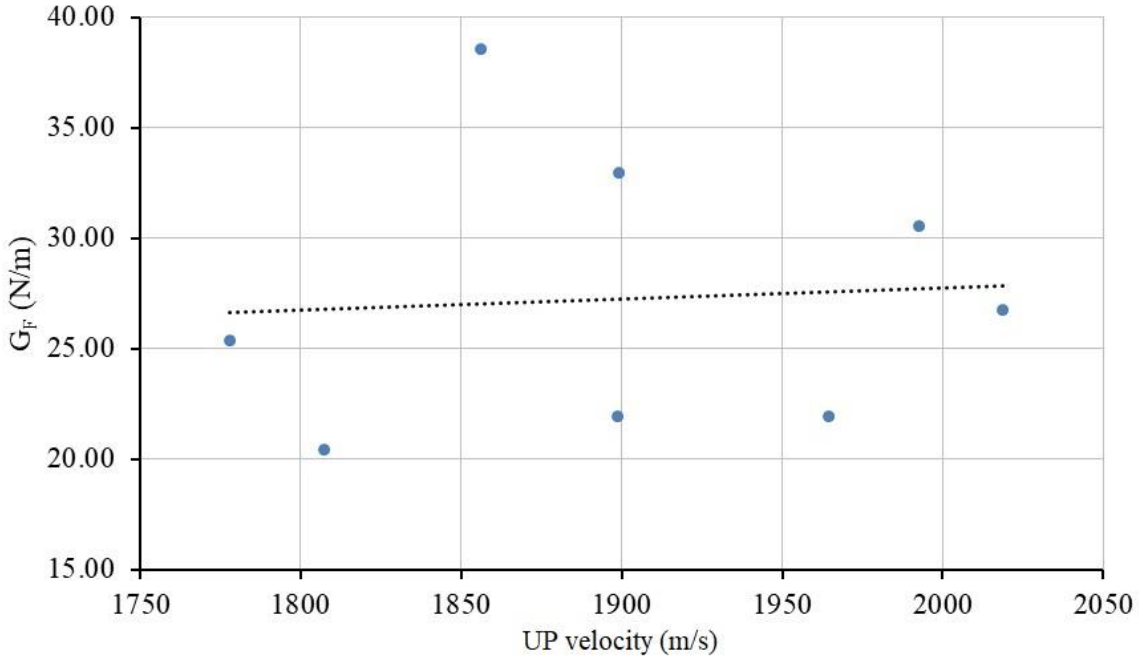

Fig. 17. Relationship between UPV (m/s) and fracture energy G_F (N/m).

Figure 17 shows the relationships between the UPV values and the fracture energy in the specimens. This figure proves that there is a relationship between the UPV and G_F values, even though the slope of the data trend line is small. Additionally, Figure 18 shows the relationships between the UPV and tensile strength values. There is a clear positive relationship between the data and a clear trend toward higher tensile strength values for higher UPV values.

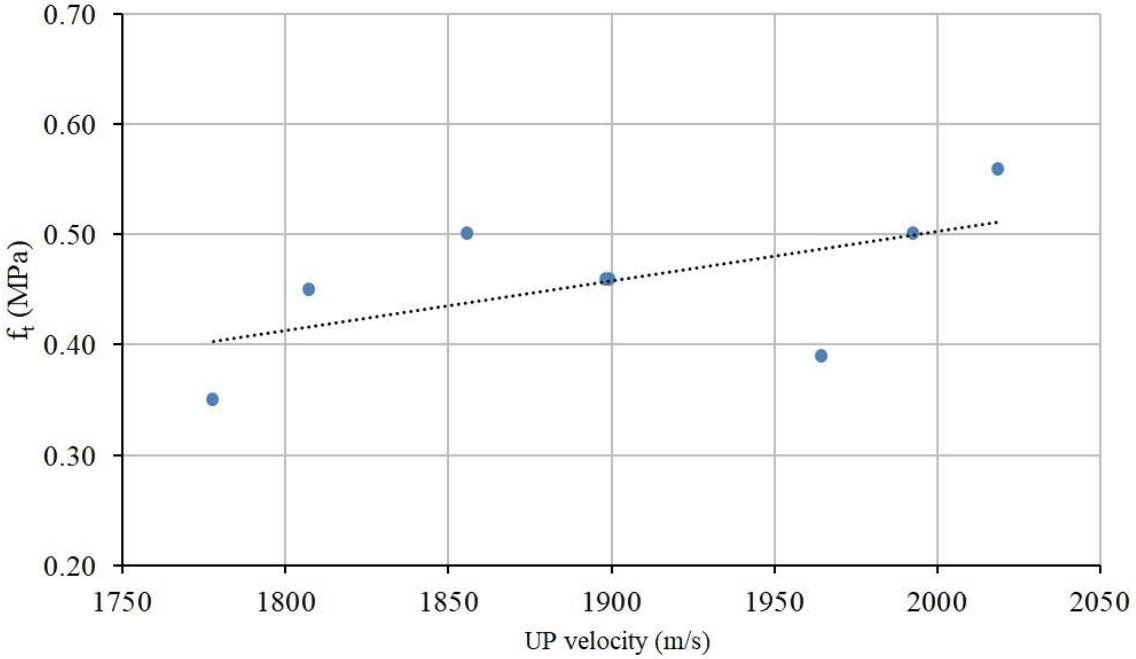

Fig. 18. Relationship between UPV (m/s) and tensile strength f_t (MPa).

5. Conclusions.

This article analyzes the fracture behavior of RE specimens manufactured in a traditional manner, with dosages and materials that imitate those of historical RE walls that are part of heritage structures. Lime was used as a stabilizer in two fixed dosages, with soil:lime ratios of 3:1 and 4:1. To characterize the materials, tests were carried out to measure the variations and final values of the density and UPV, and 3PBT tests were conducted to obtain data on the fracture energy and tensile strength.

From the results, we can conclude that the specimens achieved stable density values fifteen days after their manufacture, and from that date forward there were no variations in the UPV measurements. The mean values of the density and UPV were 1.98 gr/cm^3 and 1818.16 m/s for the 3:1 dosage and 2.01 gr/cm^3 and 1869.36 m/s for the 4:1 dosage (Table 2). It was verified that the changes in the density and UPV over time were not affected by the dosages used in the study (Figures 5 and 7). Regarding the relationship between both values, it was confirmed that the behavior was as expected, with higher propagation velocities in the densest pieces (Figure 15).

Additionally, from the results of the 3PBT fracture tests, it was verified that there was a clear correlation between the fracture energy (G_F) and tensile strength (f_t) data with the soil:lime ratio employed in the manufacture of the specimens. The increase in the G_F values for the 3:1 dosage compared with the 4:1 dosage reached 46% (table 3), and the increase in the tensile strength reached 10.18% (table 4).

Thus, the general analysis of the fracture behavior of the RE wall showed that, from a qualitative standpoint, the behavior was totally similar to that of mass concrete. For this reason, RE could be considered as a quasi-brittle material that follows Hillerborg's discrete crack model (Figures 13 and 14). The relationship between both mechanical parameters was as expected, with higher tensile strengths at higher fracture energy values (Figure 16).

Conflict of interest

There is no conflict of interest between the data provided and the funding received to acquire materials and carry out the study.

Acknowledgements

This study is part of the project PREFORTI (BIA2015 69938-R) entitled "Metodología sostenible de conservación y mantenimiento de fortificaciones medievales de tierra del sudeste de la Península Ibérica. Diagnóstico y prevención ante riesgos naturales y antrópicos" ("Sustainable methodology for the conservation and maintenance of mediaeval rammed-earth fortifications in the south-east of the Iberian Peninsula. Diagnosis and prevention against natural and anthropic risks"), financed by the Agencia Estatal de Investigación (Spanish National Research Agency) and the European Regional Development Fund.
We would also like to thank Heidelberg Cement Hispania for the donated lime NHL3.4.

References

[1] Jaquin PA, Augarde CE, Gerrard CM. Chronological description of the spatial development of rammed earth techniques. International Journal of Architectural Heritage 2008;2:377-400.

[2] Easton D. The rammed earth house. : Chelsea Green Publishing, 2007.

[3] Amendoeira AP, Fernandes M. Le patrimoine mondial en terre dans la Méditerranée. 2009.

[4] Gandreau D, Delboy L. World heritage inventory of earthen architecture. Villefontaine, CRAterre-ENSAG 2012.

[5] Ghafory-Ashtiany M, Hosseini M. Post-Bam earthquake: recovery and reconstruction. Nat Hazards 2008;44:229-41.

[6] Angulo-Ibáñez Q, Mas-Tomás Á, Galvañ-LLopis V, Sántolaria-Montesinos JL. Traditional braces of earth constructions. Constr Build Mater 2012;30:389-99.

[7] Aymat C. Patología y recuperación de fábricas de cajones de tapial. Cercha. Consejo General de la Arquitectura Técnica de España 2000:75-82.

[8] López Martínez FJ. Tapias y tapiales. Loggia, Arquitectura & Restauración 1999:74-89.

[9] Serrano S, de Gracia A, Cabeza LF. Adaptation of rammed earth to modern construction systems: Comparative study of thermal behavior under summer conditions. Appl Energy 2016;175:180-8.

[10] Habitat UN. Going Green: A Handbook Of Suistainable Housing Practice in Developing Countries. United Nations Human Settlements Program 2012.

[11] Binici H, Aksogan O, Shah T. Investigation of fibre reinforced mud brick as a building material. Construction and Building Materials 2005;19:313-8.

[12] Ciancio D, Augarde C. Capacity of unreinforced rammed earth walls subject to lateral wind force: elastic analysis versus ultimate strength analysis. Mater Struct 2013;46:1569-85.

[13] Corbin A, Augarde C. Fracture energy of stabilised rammed earth. Procedia materials science 2014;3:1675-80.

[14] Miccoli L, Müller U, Pospíšil S. Rammed earth walls strengthened with polyester fabric strips: experimental analysis under in-plane cyclic loading. Constr Build Mater 2017;149:29-36.

[15] Fagone M, Kloft H, Loccarini F, Ranocchiai G. Jute fabric as a reinforcement for rammed earth structures. Composites Part B: Engineering 2019;175:107064.

[16] Hussaini SMS, Toufigh V. Strength and Fracture Behavior of Rammed-Earth Materials. J Mater Civ Eng 2019;31:04019228.

[17] Toufigh V, Kianfar E. The effects of stabilizers on the thermal and the mechanical properties of rammed earth at various humidities and their environmental impacts. Constr Build Mater 2019;200:616-29.

[18] Liu K, Wang M, Wang Y. Seismic retrofitting of rural rammed earth buildings using externally bonded fibers. Constr Build Mater 2015;100:91-101.

[19] Miccoli L, Oliveira DV, Silva RA, Müller U, Schueremans L. Static behaviour of rammed earth: experimental testing and finite element modelling. Mater Struct 2015;48:3443-56.

[20] Mužíková B, Otcovská T, Padevět P. Determining fracture energy of unstabilised rammed earth by using three-point bending test. Experimental Stress Analysis - 56th International Scientific Conference, EAN 2018 - Conference Proceedings 2018:292-5.

[21] Shrestha KC, Aoki T, Miyamoto M, Wangmo P. In-Plane Shear Resistance between the Rammed Earth Blocks with Simple Interventions: Experimentation and Finite Element Study. Buildings 2020;10:57.

[22] Jayasinghe C, Kamaladasa N. Compressive strength characteristics of cement stabilized rammed earth walls. Constr Build Mater 2007;21:1971-6.

[23] Ciancio D, Gibbings J. Experimental investigation on the compressive strength of cored and molded cement-stabilized rammed earth samples. Constr Build Mater 2012;28:294-304.

[24] Ciancio D, Beckett C. Rammed earth construction: cutting-edge research on traditional and modern rammed earth. : CRC Press, 2015.

[25] Kariyawasam K, Jayasinghe C. Cement stabilized rammed earth as a sustainable construction material. Constr Build Mater 2016;105:519-27.

[26] Ciancio D, Beckett C, Carraro J. Optimum lime content identification for lime-stabilised rammed earth. Constr Build Mater 2014;53:59-65.

[27] Canivell J, Martin-del-Rio JJ, Alejandre FJ, García-Heras J, Jimenez-Aguilar A. Considerations on the physical and mechanical properties of lime-stabilized rammed earth walls and their evaluation by ultrasonic pulse velocity testing. Constr Build Mater 2018;191:826-36.

[28] Gamrani N, Chaham KR, Ibnoussina M, Fratini F, Rovero L, Tonietti U et al. The particular "rammed earth" of the Saadian sugar refinery of Chichaoua (XVIth century, Morocco): mineralogical, chemical and mechanical characteristics. Environmental Earth Sciences 2012;66:129-40.

[29] Martín Civantos JM. Ensayo de análisis comparativo de técnicas, materiales y tipos constructivos en las fortificaciones medievales del Zenete (Granada). Miscelánea Medieval Murciana 2001;25-26:183-229.

[30] Gutierrez-Carrillo ML, Arizzi A, Bestué Cardiel I, Sebastián Pardo E. Study of the State of Conservation and the Building Materials Used in Defensive Constructions in South-Eastern Spain: The Example of Mula Castle in Murcia. International Journal of Architectural Heritage 2019.

[31] Martín-del-Rio JJ, Flores-Alés V, Alejandre-Sánchez FJ, Blasco-López FJ. New Method for Historic Rammed-earth Wall Characterization: The Almohade Ramparts of Malaga and Seville. Studies in Conservation 2019;64:363-72.

[32] Kraus C, Hirmas D, Roberts J. Compressive strength of blood stabilized earthen architecture. Earthen Architecture: Past, Present and Future - Proceedings of the International Conference on Vernacular Heritage, Sustainability and Earthen Architecture 2015:217-20.

[33] Vénuat M. Relation entre la carbonatation du beton et les phenomenes de corrosión des armatures du beton. 1978;364:42-7.

[34] Galán I, Andrade MC, Castellote MM. Carbonatación del hormigón: combinación del CO2 con las fases hidratadas del cemento y frente de cambio de pH. Carbonatación del hormigón: combinación de CO2 con las fases hidratadas del cemento y frente de cambio de pH 2011:202.

[35] Galán-Marín C, Rivera-Gómez C, Bradley F. Ultrasonic, molecular and mechanical testing diagnostics in natural fibre reinforced, polymer-stabilized earth blocks. International Journal of Polymer Science 2013;2013.

[36] Liang R, Hota G, Lei Y, Li Y, Stanislawski D, Jiang Y. Nondestructive evaluation of historic Hakka rammed earth structures. Sustainability 2013;5:298-315.

[37] Bernat-Maso E, Teneva E, Escrig C, Gil L. Ultrasound transmission method to assess raw earthen materials. Constr Build Mater 2017;156:555-64.

[38] Ontiveros Ortega E, Sebastián Pardo E, Valverde Espinosa I, Gallego Roca FJ. Estudio de los materiales de construcción de las murallas del Albayzín (Granada). PH: boletín del Instituto Andaluz del Patrimonio Histórico 2008;16:32-47.

[39] Alejandre FJ, Martín del Río, Juan J. Caracterización analítica de la muralla de tapial almohade de San Juan de Aznalfarache (Sevilla, España). Caracterización analítica de la muralla de tapial almohade de San Juan de Aznalfarache (Sevilla, España) 2012.

[40] de la Torre López, María José. Estudio de los materiales de construcción en la Alhambra. ISBN : 8433821156 1995:219.

[41] Chatterji S. Mechanism of expansion of concrete due to the presence of dead-burnt CaO and MgO. Cem Concr Res 1995;25:51-6.

[42] Müller A, Fuhr C, Knöfel D. Frost resistance of cement mortars with different lime contents. Cem Concr Res 1995;25:809-18.

[43] Selwitz C. Saving the Fort Selden ruins: The use of a composite blend of chemicals to stabilize fragile historic adobe. Conservation and management of archaeological sites 1995;1:109-16.

[44] Cazalla O, Rodriguez Navarro C, Sebastian E, Cultrone G, De la Torre, Maria Jose. Aging of lime putty: effects on traditional lime mortar carbonation. J Am Ceram Soc 2000;83:1070-6.

[45] Cazalla O, Sebastián EM, de la Torre, María José, de Paolis M, Rodriguez-Navarro C, Cultrone G. Estudio mineralógico-petrográfico de los materiales de construcción de la Rauda en la Alhambra. Cuadernos de la Alhambra 2000:167-80.

[46] Cazalla O. Morteros de cal: aplicación en el patrimonio histórico. 2002.

[47] Ontiveros Ortega E, Valverde Espinosa I, Sebastian Pardo E. Tecnicas de analisis aplicadas al estudio de los tapiales de las murallas de Granada. 1996:270-3.

[48] RILEM DR. Determination of the fracture energy of mortar and concrete by means of three-point bend tests on notched beams. Mater Struct 1985;18:285-90.

[49] AENOR AE. UNE EN 12504-4: Testing concrete. Part 4: Determination of ultrasonic pulse velocity. Ensayos de Hormigón en Estructuras 2006.

[50] Guinea GV, Planas J, Elices M. Measurement of the fracture energy using three-point bend tests: Part 1-Influence of experimental procedures. Materials and Structures 1992;25:212-8.

[51] Planas J, Elices M, Guinea GV. Measurement of the fracture energy using three-point bend tests: Part 2-Influence of bulk energy dissipation. Materials and Structures 1992;25:305-12.

[52] Elices M, Guinea GV, Planas J. Measurement of the fracture energy using three-point bend tests: Part 3-influence of cutting the P-δ tail. Materials and Structures 1992;25:327-34.

[53] Van Balen K, Van Gemert D. Modelling lime mortar carbonation. Mater Struct 1994;27:393-8.

[54] Hillerborg A. The theoretical basis of a method to determine the fracture energy G F of concrete. Materials and Structures 1985;18:291-6.

[55] Cifuentes-Bulté H, Ríos JD, Gómez Álvarez EJ. Effect of mix design on the size-independent fracture energy of normal-and high-strength self-compacting concrete. Materiales de Construcción, 68 (329), 1-11. 2018.

TITLE: Fracture behavior of rammed earth in historic buildings

HIGHLIGHTS

- The influence of dosage on the density and ultrasonic pulse velocity of rammed earth test tubes was analyzed.
- The fracture energy and tensile strength values are related to the dosage of the specimens.
- Rammed earth could be considered as a quasi-brittle material that follows Hillerborg's discrete crack model.

Declaration of interests

☒ The authors declare that they have no known competing financial interests or personal relationships that could have appeared to influence the work reported in this paper.

☐The authors declare the following financial interests/personal relationships which may be considered as potential competing interests:
